
Heterogeneous-Modal Unsupervised Domain Adaptation via Latent Space Bridging

Jiawen Yang^{1,*}, Shuhao Chen^{1,*}, Yucong Duan², Ke Tang¹, Yu Zhang^{1,†}

¹Southern University of Science and Technology

²SZ DJI Technology Co., Ltd

Abstract

Unsupervised domain adaptation (UDA) methods effectively bridge domain gaps but become struggled when the source and target domains belong to entirely distinct modalities. To address this limitation, we propose a novel setting called Heterogeneous-Modal Unsupervised Domain Adaptation (HMUDA), which enables knowledge transfer between completely different modalities by leveraging a bridge domain containing unlabeled samples from both modalities. To learn under the HMUDA setting, we propose Latent Space Bridging (LSB), a specialized framework designed for the semantic segmentation task. Specifically, LSB utilizes a dual-branch architecture, incorporating a feature consistency loss to align representations across modalities and a domain alignment loss to reduce discrepancies between class centroids across domains. Extensive experiments conducted on six benchmark datasets demonstrate that LSB achieves state-of-the-art performance.

1 Introduction

Unsupervised domain adaptation (UDA) methods [40, 41, 42] are powerful in transferring knowledge from a labeled source domain to an unlabeled target domain, particularly when the two domains exhibit significant distributional differences. While traditional UDA methods [21, 23, 33, 34, 35] have achieved notable success in scenarios where the source and target domains share the same modality (e.g., the image modality), multi-modal UDA (a.k.a. cross-modal UDA) [36, 37, 38, 75] has been recently proposed to address a more complex task of transferring knowledge from the source domain to the target one with multiple modalities (e.g., image and 3D point cloud). However, a significant challenge arises when the source and target domains belong to entirely distinct modalities, such as transferring knowledge from 2D images to 3D point clouds.

Consider the semantic segmentation task [44, 50, 51] in real-world applications. In autonomous driving [45, 46, 47, 32], accurately segmenting objects in 3D point clouds captured by LiDAR sensors is essential for safe navigation. However, acquiring labeled 3D point cloud data is expensive and time-consuming [48]. Conversely, large-scale 2D segmentation datasets [43, 83, 84, 85] are far more abundant, and annotating 2D image data is significantly easier and more cost-effective [81]. This disparity motivates the need to transfer knowledge from labeled 2D images to improve the segmentation performance on unlabeled 3D point clouds.

Despite its importance, several challenges exist in this heterogeneous transfer [65]. First, the inherent differences in data structure and representation between modalities make it difficult to transfer knowledge directly [36, 15, 37]. For example, 2D images are dense and grid-structured, while 3D point clouds are sparse and irregular. Second, the absence of labeled data in the target domain exacerbates the difficulty of learning effective representations. Existing UDA methods, which assume

*Equal contribution †Corresponding author

the same modality/modalities for both source and target domains, are ill-suited to address these challenges.

To address those issues, we formally propose a new setting called Heterogeneous-Modal Unsupervised Domain Adaptation (HMUDA), where the source domain data (e.g., 2D images) and unlabeled target domain data (e.g., 3D point clouds) belong to different modalities. As unlabeled data can be easily obtained [49], HMUDA assumes the existence of a bridge domain containing unlabeled samples with both source and target modalities. The HMUDA setting is visually depicted in Figure 1, and Table 1 provides a comparative analysis, highlighting its differences from existing domain adaptation (DA) paradigms, including UDA, multi-modal UDA (MM-UDA), and heterogeneous domain adaptation (HDA) [52, 53]. Then, we propose Latent Space Bridging (LSB), a novel HMUDA framework specifically designed for semantic segmentation tasks. Specifically, the proposed LSB method employs a dual-branch architecture, comprising a source network and a target network tailored for the source and target modalities, respectively. Those networks are trained to perform pointwise segmentation using the source data with ground truth labels and the bridge data with pseudo labels. To enhance the feature alignment, we propose a **feature consistency loss** to encourage similar feature representations for samples with both modalities in the bridge domain and a **domain alignment loss** to minimize discrepancies between class centroids in the source and target domains. Experimental results across various benchmark datasets demonstrate that the proposed LSB method effectively transfers knowledge from the source domain to the target domain, outperforming both the source-only method and existing UDA methods by a significant margin.

Our contributions are summarized as follows.

- We introduce a new DA setting, heterogeneous-modal unsupervised domain adaptation, to facilitate knowledge transfer between heterogeneous modalities.
- We propose the Latent Space Bridging method, a tailored solution for the semantic segmentation task under the HMUDA setting.
- Extensive experiments on benchmark datasets demonstrate the effectiveness of the proposed LSB method, showcasing its ability to outperform existing methods.

2 Related Work

2.1 Unsupervised Domain Adaptation

Unsupervised domain adaptation (UDA) [80] aims to transfer knowledge from a labeled source domain to an unlabeled target domain, addressing the challenge of the domain shift. Traditional UDA methods [21, 55, 54, 56] have achieved significant success in various applications by aligning the feature distributions between the source and target domains. For instance, discrepancy-based methods such as DAN [21] and CORAL [55] minimize the statistical distance between source and target feature distributions. Meanwhile, adversarial-based methods like DANN [56] and ADDA [57] employ adversarial training to learn domain-invariant features, leveraging a domain classifier to ensure that extracted features cannot be distinguished as originating from either the source or target domain.

In semantic segmentation, UDA methods have been extended to tackle the pixel-level alignment challenge. Many of these methods also employ adversarial training for aligning the two domains. For instance, CyCADA [29] uses cycle-consistent adversarial networks to adapt both the pixel and feature levels. AdaptSegNet [58] incorporates adversarial training at the output space to align the segmentation maps. Recently, CLAN [33] and CoSMix [34] further refine the adversarial approach by focusing on class-level alignment and contextual consistency. However, adversarial training can be unstable and a high computational burden for segmentation tasks [74]. Different from them, the proposed LSB method uses discrepancy-based feature alignment, which directly minimizes the difference between source and target feature distributions.

2.2 Multi-Modal Domain Adaptation

Multi-modal domain adaptation [36, 37, 75, 76] involves transferring knowledge across domains with multiple modalities, such as images and text, or images and 3D point clouds. This approach leverages the complementary information from different modalities to enhance the adaptation performance.

For example, Jaritz et al. introduce xMUDA [36], a cross-modal learning method that combines RGB images and LiDAR point clouds for improving 3D semantic segmentation accuracy. DsCML [37] employs adversarial learning at the output level to model domain-invariant representations. SSE-xMUDA [75] presents a self-supervised exclusive learning mechanism that exploits the unique information of different modalities to complement each other. Dual-Cross [28] designs a multi-modal stylized transfer module to alleviate the domain shift problem. These existing methods assume that both the source and target domains contain multi-modal data, and typically, adaptation only occurs between the same type of modal data. In contrast, our approach introduces a novel setting where both the source and target domains contain only one type of modality. To bridge the modal gap, we introduce an unlabeled bridge domain that possesses both source and target modalities.

2.3 Heterogeneous Domain Adaptation

Heterogeneous domain adaptation (HDA) addresses the adaptation between domains with different feature spaces or data types, presenting unique challenges due to inherent differences in feature representations. HDA methods can be divided into two categories: symmetric transformations [62, 63, 68, 53, 69] and asymmetric transformations [72, 70, 79, 78]. Symmetric transformation methods, like HFA [62] and JGSA [63], involve projecting both source and target domains into a common latent space for alignment. This approach facilitates a balanced representation by leveraging complementary information from both domains. In contrast, asymmetric transformation methods [72] focus on transforming one domain to align with the other. Although effective, most HDA methods require partial target domain labels for guiding the adaptation process [72, 62], especially when aligning feature spaces [77]. Moreover, the majority of HDA methods are not end-to-end, which necessitates separate stages for feature extraction and alignment [53]. In contrast, our approach is both end-to-end and label-free in the target domain, simultaneously training networks for both modalities.

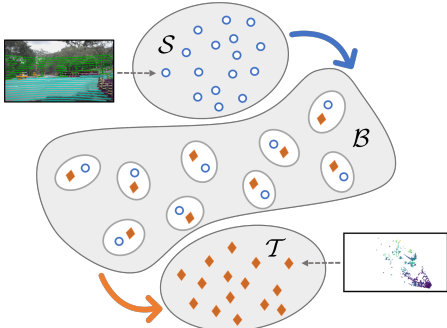


Figure 1: The illustration of HMUDA setting.

Table 1: The comparison between HMUDA and other DA settings. The \mathcal{M}_1 and \mathcal{M}_2 represent different modalities, ‘E-to-E’ indicates whether the corresponding setting uses the end-to-end training strategy, and ‘Ex-Label’ indicates whether the corresponding setting uses extra labeled target data.

	Source		Target		E-to-E	Ex-Label
	\mathcal{M}_1	\mathcal{M}_2	\mathcal{M}_1	\mathcal{M}_2		
UDA	✓	✗	✓	✗	✓	✗
MM-UDA	✓	✓	✓	✓	✓	✗
HDA	✓	✗	✗	✓	✗	✓
HMUDA	✓	✗	✗	✓	✓	✗

3 Problem Formulation for HMUDA

In this section, we introduce the HMUDA setting. Under the HMUDA setting, there exists a labeled source domain $\mathcal{S} = \{(\mathbf{x}^s, \mathbf{y}^s)\}$, where each sample consists of an input $\mathbf{x}^s \in \mathcal{M}_1$ and pointwise segmentation labels $\mathbf{y}^s \in \mathbb{R}^{C \times N}$ for \mathbf{x}^s . Here, \mathcal{M}_1 denotes the source modality of the input (e.g., the 2D image), N is the number of labeled points in the input for semantic segmentation, and C is the number of classes in the semantic segmentation task. Moreover, there exists an unlabeled target domain $\mathcal{T} = \{\mathbf{x}^t\}$, where \mathbf{x}^t belongs to a different modality \mathcal{M}_2 (e.g., the 3D point cloud). Additionally, we assume the existence of an unlabeled bridge domain $\mathcal{B} = \{(\mathbf{x}^{bs}, \mathbf{x}^{bt})\}$, where $\mathbf{x}^{bs} \in \mathcal{M}_1$ and $\mathbf{x}^{bt} \in \mathcal{M}_2$ are from the two modalities and correspond to the same input. Note that the bridge domain could differ from the source and target domains. Under the HMUDA setting, we aim to transfer the knowledge in \mathcal{S} to help the learning of \mathcal{T} with the help of the bridge domain \mathcal{B} . In the following, we give the definition for HMUDA.

Definition 1. (HMUDA) *Heterogeneous Modality Unsupervised Domain Adaptation (HMUDA) transfers knowledge from a labeled source domain \mathcal{S} to an unlabeled target domain \mathcal{T} across different modalities. This transfer is facilitated by an unlabeled bridge domain \mathcal{B} , which provides paired*

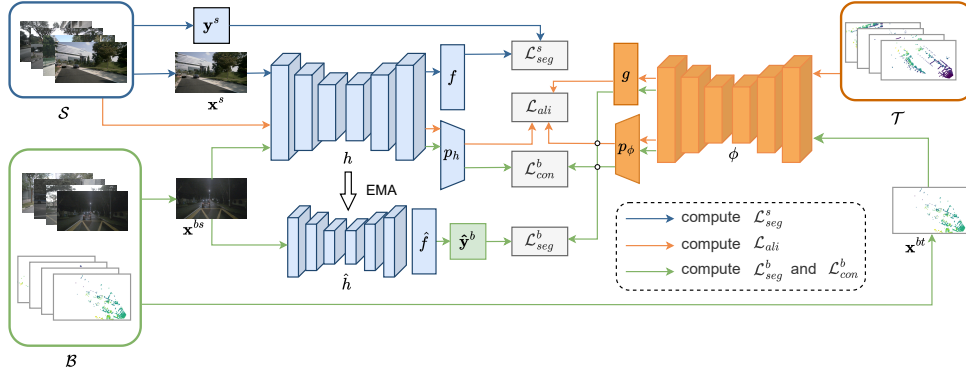


Figure 2: An illustration of the proposed LSB framework. \mathcal{S} , \mathcal{T} , and \mathcal{B} denote the source, target, and bridge domains, respectively. \mathbf{x}^s , \mathbf{x}^{bs} and \mathbf{x}^{bt} represent samples from each corresponding domain. Lines within different colors denote the data flow for computing different losses.

samples from both source and target modalities. The objective of HMUDA is to leverage the labeled data from \mathcal{S} and the paired data in \mathcal{B} to improve the learning and performance on the target domain \mathcal{T} .

As shown in Table 1, HMUDA differs from existing DA settings. Specifically, unsupervised domain adaptation (UDA) addresses the domain gap between source and target domains within the same modality. Multi-modal UDA (MM-UDA) assumes the existence of different modalities for both source and target domains. Heterogeneous domain adaptation (HDA) transfers knowledge from the source domain to the target domain with homogeneous or heterogeneous modalities but usually requires extra labeled target data. Moreover, HDA manually extracts features from the original data without learning the feature extractors and hence it does not support end-to-end training. Compared with UDA and MM-UDA, HMUDA considers a more complex scenario involving heterogeneous source and target modalities. Different from HDA, HMUDA supports the end-to-end training without requiring additional labeled target data, making it more streamlined and practical than HDA.

4 Methodology

In this section, we present the proposed LSB method for HMUDA. We introduce the entire architecture of the proposed LSB method in Section 4.1. Then, we introduce the losses in LSB to learn to bridge the source and target model by the bridge domain (Section 4.2) and align class centroids across domains (Section 4.3). Next, we give the entire objective function and the algorithm for the LSB method in Section 4.4. Finally, Section 4.5 provides a theoretical analysis of the error bound under the HMUDA setting.

4.1 Architecture

As depicted in Figure 2, the proposed LSB method employs a dual-branch architecture to predict pointwise segmentation labels. The architecture in the LSB method consists of two distinct segmentation networks: (i) a **source network** $\{h, f\}$ tailored for the source modality \mathcal{M}_1 with a feature extractor $h(\cdot) : \mathcal{M}_1 \rightarrow \mathbb{R}^{d_h \times N}$ and a classifier $f(\cdot) : \mathbb{R}^{d_h \times N} \rightarrow \mathbb{R}^{C \times N}$, where d_h is the feature dimension of h . (ii) a **target network** $\{\phi, g\}$ designed for the target modality \mathcal{M}_2 with a feature extractor $\phi(\cdot) : \mathcal{M}_2 \rightarrow \mathbb{R}^{d_\phi \times N}$ and a classifier $g(\cdot) : \mathbb{R}^{d_\phi \times N} \rightarrow \mathbb{R}^{C \times N}$, where d_ϕ is the feature dimension of ϕ .

During training, the source domain and bridge domain data associated with modality \mathcal{M}_1 are input into the source network, while the target and bridge domain data belonging to modality \mathcal{M}_2 are input into the target network. Both the source and target networks can predict the pointwise segmentation labels independently. For example, given a target input \mathbf{x}^t , the target model generates the probability distribution of N points over C classes as $g(\phi(\mathbf{x}^t))$. Further implementation details are provided in Section. 5.1.

4.2 Bridging Source and Target Networks

To train the source network, a natural solution is to minimize the cross-entropy loss between the prediction of input \mathbf{x}^s (i.e., $f(h(\mathbf{x}^s))$) and its corresponding labels \mathbf{y}^s . This segmentation loss, denoted by $\mathcal{L}_{\text{seg}}^s$, is formally defined as

$$\mathcal{L}_{\text{seg}}^s(\mathbf{x}^s, \mathbf{y}^s) = -\frac{1}{N} \sum_{i=1}^N (\mathbf{y}_{:,i}^s)^\top \log(f(h(\mathbf{x}^s))), \quad (1)$$

where $\mathbf{y}_{:,i}^s$ represents the i -th column of \mathbf{y}^s corresponding to the one-hot label for the i -th segment point.

Similarly, one can train the target network using the segmentation loss based on the target input \mathbf{x}^t and its corresponding labels. However, since labels for the target domain samples are unavailable, directly training the target network becomes infeasible. To address this issue, we use the bridge domain instead to train the target network. Specifically, we introduce a teacher source model, comprising \hat{f} and \hat{h} , which are updated from f and h using the exponential moving average (EMA) [16] at each iteration as

$$\boldsymbol{\theta}_{\hat{f}} \leftarrow \alpha \boldsymbol{\theta}_{\hat{f}} + (1 - \alpha) \boldsymbol{\theta}_f, \quad \boldsymbol{\theta}_{\hat{h}} \leftarrow \alpha \boldsymbol{\theta}_{\hat{h}} + (1 - \alpha) \boldsymbol{\theta}_h, \quad (2)$$

where $\boldsymbol{\theta}_f$, $\boldsymbol{\theta}_h$, $\boldsymbol{\theta}_{\hat{f}}$ and $\boldsymbol{\theta}_{\hat{h}}$ denotes the parameters of f , h , \hat{f} , \hat{h} , respectively. α is a hyperparameter that is dynamically adjusted during training as

$$\alpha = \min\left(1 - \frac{1}{t+1}, \alpha\right), \quad (3)$$

where t denotes the number of training iterations completed so far. The pseudo-label $\hat{\mathbf{y}}^b$ for the sample pair $(\mathbf{x}^{bs}, \mathbf{x}^{bt})$ in the bridge domain \mathcal{B} is generated by the teacher source network as

$$\hat{\mathbf{y}}^b = \text{one-hot}\left(\arg \max \hat{f}(\hat{h}(\mathbf{x}^{bs}))\right), \quad (4)$$

where $\text{one-hot}(\cdot)$ denotes the transformation that converts the prediction into the one-hot vector. Then, we propose the loss $\mathcal{L}_{\text{seg}}^b$ to train the target network on the bridge domain \mathcal{B} as

$$\mathcal{L}_{\text{seg}}^b(\mathbf{x}^{bs}, \mathbf{x}^{bt}) = -\frac{1}{N} \sum_{i=1}^N (\hat{\mathbf{y}}_{:,i}^b)^\top \log(g(\phi(\mathbf{x}^{bt}))), \quad (5)$$

where $\hat{\mathbf{y}}_{:,i}^b$ denotes the i -th column of $\hat{\mathbf{y}}^b$ corresponding to the one-hot pseudo label for the i -th segment point.

For an input sample pair $(\mathbf{x}^{bs}, \mathbf{x}^{bt})$, the source and target networks should extract similar features since they share the same labels. To encourage the consistent features between the source and target networks, we introduce learnable projections $p_h : \mathbb{R}^{d_h \times N} \rightarrow \mathbb{R}^{d \times N}$ and $p_\phi : \mathbb{R}^{d_\phi \times N} \rightarrow \mathbb{R}^{d \times N}$, which map the source and target feature into a d -dimensional shared feature space, respectively. To minimize the discrepancy between the projected features of the source and target networks, we define the feature consistency loss $\mathcal{L}_{\text{con}}^b$ as

$$\mathcal{L}_{\text{con}}^b(\mathbf{x}^{bs}, \mathbf{x}^{bt}) = \frac{1}{N} \sum_{i=1}^N \left(\|p_h(h(\mathbf{x}^{bs})) - p_\phi(\phi(\mathbf{x}^{bt}))\|_2^2 + \lambda_w \|\mathbf{w}\|_2^2 \right), \quad (6)$$

where $\|\cdot\|_2$ denotes the ℓ_2 norm of a vector and $\lambda_w > 0$ is a hyper-parameter controlling the strength of the regularization term $\|\mathbf{w}\|_2^2$, which is applied to parameters in p_h and p_ϕ .

4.3 Cross-Modal Domain Alignment

Directly training the models using the source and bridge domain often leads to overfitting[54], resulting in diminished performance on the target domain. To alleviate this problem, inspired by the discrepancy-based UDA methods [21, 22], we learn the representation that minimizes the distance between the source and target domains. To begin with, we obtain the pseudo label $\hat{\mathbf{y}}^t$ for each $\mathbf{x}^t \in \mathcal{T}$

by the target network. For class c , we define the class centroid features $\mathbf{m}_c^s \in \mathbb{R}^d$ for the source domain and $\mathbf{m}_c^t \in \mathbb{R}^d$ for the target domain as

$$\mathbf{m}_c^s = \left(\sum_{(\mathbf{x}^s, \mathbf{y}^s) \in \mathcal{S}} \mathbf{y}_c^s \mathbf{1} \right)^{-1} \sum_{(\mathbf{x}^s, \mathbf{y}^s) \in \mathcal{S}} p_h(h(\mathbf{x}^s)) (\mathbf{y}_c^s)^\top \quad (7)$$

$$\mathbf{m}_c^t = \left(\sum_{\mathbf{x}^t \in \mathcal{T}} \hat{\mathbf{y}}_c^t \mathbf{1} \right)^{-1} \sum_{\mathbf{x}^t \in \mathcal{T}} p_\phi(\phi(\mathbf{x}^t)) (\hat{\mathbf{y}}_c^t)^\top, \quad (8)$$

where \mathbf{y}_c^s and $\hat{\mathbf{y}}_c^t$ denote the c -th row element of \mathbf{y}^s and $\hat{\mathbf{y}}^t$, respectively, and $\mathbf{1}$ denotes an N dimension vector where all elements equal to one. We expect the source and target models to share similar centroid features for each class. To this end, we minimize the discrepancy between the centroids using the alignment loss \mathcal{L}_{ali} as

$$\mathcal{L}_{\text{ali}}(\mathcal{S}, \mathcal{T}) = \frac{1}{C} \sum_{c=1}^C 1 - \cos(\mathbf{m}_c^s, \mathbf{m}_c^t), \quad (9)$$

where $\cos(\cdot)$ denotes the cosine similarity function.

4.4 Objective Function and Algorithm

We jointly learn the source and target networks by minimizing the final objective $\mathcal{L}(\mathcal{S}, \mathcal{B}, \mathcal{T})$, which combines $\mathcal{L}_{\text{seg}}^s$, $\mathcal{L}_{\text{seg}}^b$, \mathcal{L}_{con} and \mathcal{L}_{ali} together, i.e.,

$$\mathcal{L}(\mathcal{S}, \mathcal{B}, \mathcal{T}) = \sum_{(\mathbf{x}^s, \mathbf{y}^s) \in \mathcal{S}} \left(\mathcal{L}_{\text{seg}}^s(\mathbf{x}^s, \mathbf{y}^s) \right) + \lambda_a \mathcal{L}_{\text{ali}}(\mathcal{S}, \mathcal{T}) + \sum_{(\mathbf{x}^{bs}, \mathbf{x}^{bt}) \in \mathcal{B}} \left(\mathcal{L}_{\text{seg}}^b(\mathbf{x}^{bs}, \mathbf{x}^{bt}) + \lambda_c \mathcal{L}_{\text{con}}^b(\mathbf{x}^{bs}, \mathbf{x}^{bt}) \right), \quad (10)$$

where $\lambda_c > 0$ and $\lambda_a > 0$ are hyperparameters to balance different losses. The overall algorithm for the LSB method is provided in Appendix A.

4.5 Theoretical Analysis

In this section, we analyze the error bound of HMUDA. Let $\mathcal{E}_s(\{h, f\}) = \mathbb{E}_{(\mathbf{x}, \mathbf{y}) \sim \mathcal{D}_s} [f(h(\mathbf{x})) \neq \mathbf{y}]$ and $\mathcal{E}_t(\{\phi, g\}) = \mathbb{E}_{(\mathbf{x}, \mathbf{y}) \sim \mathcal{D}_t} [g(\phi(\mathbf{x})) \neq \mathbf{y}]$ denote the expected error in the source domain with data distribution \mathcal{D}_s and target domain with data distribution \mathcal{D}_t , respectively. For bridge domain distribution \mathcal{D}_b , let $\mathcal{E}_{bs}(\{h, f\}) = \mathbb{E}_{(\mathbf{x}^{bs}, \mathbf{x}^{bt}, \mathbf{y}) \sim \mathcal{D}_b} [f(h(\mathbf{x}^{bs})) \neq \mathbf{y}]$ and $\mathcal{E}_{bt}(\{\phi, g\}) = \mathbb{E}_{(\mathbf{x}^{bs}, \mathbf{x}^{bt}, \mathbf{y}) \sim \mathcal{D}_b} [g(\phi(\mathbf{x}^{bt})) \neq \mathbf{y}]$ be the errors corresponding to the source and target modalities within the bridge domain. We denote the hypothesis space for the source network $\{h, f\}$ and target network $\{\phi, g\}$ as \mathcal{H}_s and \mathcal{H}_t , respectively. The optimized source and target networks are defined as follows.

Definition 2. *The ideal joint hypothesis for source and target modality is the hypothesis that minimizes the combined errors:*

$$\{h^*, f^*\} = \arg \min_{\{h, f\} \in \mathcal{H}_s} \mathcal{E}_s(\{h, f\}) + \mathcal{E}_{bs}(\{h, f\}); \quad (11)$$

$$\{\phi^*, g^*\} = \arg \min_{\{\phi, g\} \in \mathcal{H}_t} \mathcal{E}_{bt}(\{\phi, g\}) + \mathcal{E}_t(\{\phi, g\}). \quad (12)$$

The combined error for source and target modality under the ideal hypothesis are denoted as:

$$\lambda_s = \mathcal{E}_s(\{h^*, f^*\}) + \mathcal{E}_{bs}(\{h^*, f^*\}); \quad \lambda_t = \mathcal{E}_{bt}(\{\phi^*, g^*\}) + \mathcal{E}_t(\{\phi^*, g^*\}). \quad (13)$$

Moreover, similar to [86], we assume the error gap between modalities of the same domain is bounded by their feature gap as $|\mathcal{E}_{bt}(\{\phi, g\}) - \mathcal{E}_{bs}(\{h, f\})| \leq L \mathbb{E}_{(\mathbf{x}^{bs}, \mathbf{x}^{bt}) \sim \mathcal{D}_b} (d(h(\mathbf{x}^{bs}), \phi(\mathbf{x}^{bt})))$, where L is a constant and d is the distance function (e.g., the ℓ_1 distance). We are now ready to give a bound on the expected error of the target domain in the following theorem.¹

¹The proof can be found in Appendix B.

Theorem 1. For every $\{\phi, g\} \in \mathcal{H}_t$, the target domain error is bounded as:

$$\begin{aligned} \mathcal{E}_t(\{\phi, g\}) \leq & \mathcal{E}_s(\{h, f\}) + L\mathbb{E}_{(\mathbf{x}^{bs}, \mathbf{x}^{bt}) \sim \mathcal{D}_b} (d(h(\mathbf{x}^{bs}), \phi(\mathbf{x}^{bt}))) + (\lambda_s + \lambda_t) \\ & + \frac{1}{2}d_{\mathcal{H}_s \Delta \mathcal{H}_s}(\mathcal{D}_s, \mathcal{D}_b) + \frac{1}{2}d_{\mathcal{H}_t \Delta \mathcal{H}_t}(\mathcal{D}_b, \mathcal{D}_t), \end{aligned} \quad (14)$$

where $d_{\mathcal{H}_s \Delta \mathcal{H}_s}$, $d_{\mathcal{H}_t \Delta \mathcal{H}_t}$ are the $\mathcal{H}\Delta\mathcal{H}$ -distance [82] between domains in the source and target modality, respectively.

Theorem 1 shows that the target domain error is upper-bounded by the summation of five terms: (i) the source domain error $\mathcal{E}_s(\{h, f\})$; (ii) the modality discrepancy in the bridge domain; (iii) the ideal combined errors, which are a constant; (iv) the domain discrepancy between the source and bridge domains; (v) The domain discrepancy between bridge and target domains. In LSB, term (i) is optimized by using the segmentation loss defined in Eq. (1). Notably, term (ii) directly aligns with Eq. (6), which minimizes the feature gap between modalities. Moreover, Eq. (5) assesses term (iv), and Eq. (9) measures both terms (iv) and (v). Hence, the design of the LSB method aligns with the generalization bound in Theorem 1, which gives theoretical support for the proposed LSB method.

5 Experiments

In this section, we empirically evaluate the proposed LSB method under the HMUDA setting.

5.1 Experimental Settings

Datasets. We conduct experiments on several publicly available multimodal datasets, including (i) nuScenes-lidarseg [8], which is divided into different scene layouts (i.e., *USA* and Singapore (*Sing.*)) and lighting conditions (i.e., *Day* and *Night*). (ii) *A2D2* [12], which consists of data collected from Audi, featuring diverse driving scenarios with multi-sensor data. (iii) SemanticKITTI (*Sem.*) [10], a large-scale dataset providing dense pointwise semantic annotations for LiDAR scans, capturing urban environments in various driving conditions. (iv) VirtualKITTI (*Virt.*) [9], a synthetic dataset generated from realistic 3D simulations with precise ground truth annotations. To evaluate the proposed method under HMUDA, we construct six transfer tasks under the HMUDA setting, including: (i) *USA*→*Sing.* for changes in scene layout. (ii) *Day*→*Night* for changes in light conditions. (iii) *Virt*→*A2D2* and (iv) *Virt*→*Sem.* for synthetic to real data. (v) *Sem.*→*A2D2* and (vi) *A2D2*→*Sem.* for different camera setups. For the (i-iv) tasks, we use *Sem.* and *A2D2* as the bridge domain, while for the (v) and (vi) tasks, *Virt.* is used instead. In all datasets, the LiDAR and RGB cameras are synchronized and calibrated. Following [15], we only use the front camera’s images in all datasets for consistency. To evaluate the generality of HMUDA, we also perform experiments on the reverse transfer task, from 3D point clouds to 2D images. Further dataset details are provided in Appendix C.

Implement Details. By following [15], for the 2D network, we use a U-Net [18] with a ResNet34 [19] encoder pre-trained on ImageNet [17]. For the 3D network, we use the SparseConvNet[20] and U-Net[18] architectures with a voxel size of 5cm. Furthermore, we use a linear layer for projections p_ϕ and p_h , respectively. Training is conducted using the Adam optimizer with a batch size of 16, an initial learning rate of 0.001, $\beta_1 = 0.9$, and $\beta_2 = 0.999$. All the parameters are trained for 50,000 steps, with a learning rate scheduler following [36]. The hyper-parameters α is initially set to 0.999. The parameters λ_w , λ_c , and λ_a are set to 0.01, 4.0, and 0.1, respectively. We use the mean Intersection over Union (mIoU) to evaluate the performance. All experiments are conducted on an NVIDIA V100 (32GB) GPU.

Baselines. We compare the proposed LSB method with the following baselines: (i) **Oracle**: it trains the target network g, ϕ using segmentation loss on the labeled target domain $\{(\mathbf{x}^t, \mathbf{y}^t)\}$, where each input \mathbf{x}^t has a ground-truth label \mathbf{y}^t . The Oracle method serves as the upper bound for HMUDA. Both (ii) and (iii) follow a two-step pipeline: pseudo-labels are first generated by the source network on the bridge domain, and then used to train the target model. (ii) **Source-only**: the source network is trained exclusively on the source domain \mathcal{S} , and the target network is trained exclusively on the bridge domain \mathcal{B} . (iii) **Pseudo-labeling (PL)** [23]: a uni-model method employs a two-stage pseudo-label training strategy. The PL is implemented as described in [15].

Table 2: Testing mIoU results on HMUDA tasks. The best performance, excluding Oracle, is in **bold**.

	Method	\mathcal{B}	USA	Day	Virt.	\mathcal{B}	USA	Day	Virt.	\mathcal{B}	Sem.	A2D2
			→ Sing.	→ Night	→ A2D2		→ Sing.	→ Night	→ Sem.		→ A2D2	→ Sem.
D→3D	Oracle	Sem.	77.69	73.71	71.50	A2D2	77.69	73.71	82.75	Virt.	71.50	82.75
	Source-Only		51.04	57.32	19.00		49.21	55.96	36.44		43.75	43.28
	PL		52.08	59.33	16.84		55.39	61.95	46.49		39.66	38.25
	LSB		56.41	62.25	33.37		57.13	63.15	45.43		46.34	47.22
D→2D	Oracle	Sem.	76.28	62.63	85.67	A2D2	76.28	62.63	87.19	Virt.	85.67	87.19
	Source-Only		43.80	17.69	42.56		38.99	25.02	42.22		31.48	20.06
	PL		43.89	26.55	43.37		34.97	22.67	38.75		14.45	34.27
	LSB		45.35	33.81	47.92		39.83	38.36	38.03		32.49	39.89

Table 3: Effect of losses \mathcal{L}_{seg}^s , \mathcal{L}_{seg}^t , \mathcal{L}_{con}^b , and \mathcal{L}_{ali} in terms of mIoU for 2D-to-3D HMUDA tasks. The best performance is in **bold**.

\mathcal{L}_{seg}^s	\mathcal{L}_{seg}^b	\mathcal{L}_{con}^b	\mathcal{L}_{ali}	\mathcal{B}	USA → Sing.	Day → Night	Virt. → A2D2	\mathcal{B}	Sem. → A2D2
✓	✓	✗	✗	Sem.	53.62	61.86	22.72	Virt.	42.47
✓	✓	✓	✗		52.68	61.12	28.24		45.27
✓	✓	✗	✓		54.34	60.86	27.96		46.37
✓	✓	✓	✓		56.41	62.25	33.37		46.34
\mathcal{L}_{seg}^s	\mathcal{L}_{seg}^b	\mathcal{L}_{con}^b	\mathcal{L}_{ali}	\mathcal{B}	USA → Sing.	Day → Night	Virt. → Sem.	\mathcal{B}	A2D2 → Sem.
✓	✓	✗	✗	A2D2	49.35	60.64	35.74	Virt.	42.29
✓	✓	✓	✗		50.50	62.72	36.53		42.46
✓	✓	✗	✓		54.49	62.87	38.55		46.95
✓	✓	✓	✓		57.13	63.15	45.43		47.22

5.2 Main Results

Table 2 shows the testing mIoU results on HMUDA tasks. As can be seen, the LSB achieves the highest mIoU across all tasks except for *Virt.*→*Sem.*. For instance, on the 2D-to-3D task of *Day.*→*Night.* with bridge domain *A2D2*, LSB surpasses Source-Only and PL by a large margin of 5.37 and 4.33, validating its effectiveness in addressing the heterogeneous domain gaps. LSB achieves average mIoU improvements of 5.16 and 7.10 over PL across all the 2D-to-3D and 3D-to-2D tasks, respectively, demonstrating its capability to bridge source and target networks through joint training. Notably, on the 2D-to-3D task *Virt.*→*A2D2*, LSB achieves an mIoU of 33.37, outperforming Source-Only and PL by 14.37 and 16.53, respectively. This significant improvement shows the advantage of LSB in addressing substantial domain gaps. Despite these improvements, all methods under HMUDA still fall short of the Oracle, underscoring the challenges inherent in HMUDA tasks.

5.3 Ablation Studies

Effect of Different Losses \mathcal{L}_{seg}^s , \mathcal{L}_{seg}^t , \mathcal{L}_{con}^b , and \mathcal{L}_{ali} . We conduct experiments on HMUDA tasks to study the effect of losses \mathcal{L}_{seg}^s , \mathcal{L}_{seg}^t , \mathcal{L}_{con}^b , and \mathcal{L}_{ali} w.r.t. mIoU. Specifically, we consider four combinations: (i) with the two segmentation losses \mathcal{L}_{seg}^s , \mathcal{L}_{seg}^b only (i.e., LSB (w/ seg only)); (ii) without the alignment loss \mathcal{L}_{ali} (i.e., LSB (w/o \mathcal{L}_{ali})); (iii) without the consistent loss \mathcal{L}_{con}^b (i.e., LSB (w/o \mathcal{L}_{con}^b)); (iv) with all the proposed losses \mathcal{L}_{seg}^s , \mathcal{L}_{seg}^b , \mathcal{L}_{con}^b and \mathcal{L}_{ali} together (i.e. the proposed LSB). Since the two segmentation losses (i.e., \mathcal{L}_{seg}^s and \mathcal{L}_{seg}^b) are necessary for training the source and target model, we do not remove them in any variant of HMUDA.

Table 3 shows the testing mIoU results on the 2D-to-3D HMUDA tasks for different variants of LSB. As can be seen, LSB achieves the best mIoU across all HMUDA tasks, except for *Sem.*→*A2D2*. LSB outperforms LSB (w/o \mathcal{L}_{con}^b) by a large margin of 3.97 on average, validating that encouraging the consistent features benefits the learning of the target domain. Compared with LSB (w/o \mathcal{L}_{ali} , LSB achieves an average improvement of 2.36, showing the effectiveness of minimizing the distance of class centroid features between source and target domain. Moreover, LSB (w/ seg only) surpasses the previous SOTA UDA method (PL in Table 2) by 1.19 on average, demonstrating the superiority of the joint training strategy.

Effect of p_h and p_ϕ . In Sections 4.2 and 4.3, we introduce two learnable projections to map the source and target feature into a d -dimensional shared feature space. To study the effect of these two projections, we compare LSB with its variants: (i) LSB (w/o p_h), which uses a linear layer to map the target feature into the d_h -dimensional source feature space. (ii) LSB (w/o p_ϕ), which uses a linear layer to map the source feature into the d_ϕ -dimensional target feature space.

Table 4 shows the testing mIoU for $USA \rightarrow Sing.$, $Day \rightarrow Night$, and $A2D2 \rightarrow Sem.$ 2D-to-3D tasks. As can be seen, LSB consistently outperforms LSB (w/o p_ϕ) and LSB (w/o p_h) across all the tasks, validating that aligning source and target feature in a common latent space helps effective transfer. Notably, LSB (w/o p_ϕ) performs significantly worse, indicating that directly aligning features in the target feature space hinders segmentation learning.

Table 4: Effect of p_ϕ and p_h on three 2D-to-3D HMUDA tasks.

Method	\mathcal{B}	$USA \rightarrow Sing.$	$Day \rightarrow Night$	\mathcal{B}	$A2D2 \rightarrow Sem.$
LSB (w/o p_ϕ)	A2D2	20.78	3.82	Virt.	15.00
LSB (w/o p_h)		40.47	43.10		32.52
LSB		57.13	63.15		47.22

Table 5: Effect of cross-modal alignment on three 2D-to-3D HMUDA tasks.

Method	\mathcal{B}	$USA \rightarrow Sing.$	$Day \rightarrow Night$	\mathcal{B}	$A2D2 \rightarrow Sem.$
LSB (w. $\mathcal{L}_{ali}(\mathcal{B}, \mathcal{T})$)	A2D2	50.86	60.12	Virt.	44.44
LSB		57.13	63.15		47.22

Effect of cross-modal alignment. We study the effect of cross-modal domain alignment between the source and target domain on the HMUDA tasks. Instead of aligning the target domain with the source domain in Section 4.3, we conduct an additional experiment, i.e., LSB (aligns \mathcal{T} with \mathcal{B}), by minimizing the class centroid feature of the target network between the bridge and target domain. These class centroid features are computed using pseudo labels for the bridge and target domain samples. As shown in Table 5, LSB consistently outperforms LSB (aligns \mathcal{T} with \mathcal{B}), indicating that aligning the target domain with the source domain is more effective.

5.4 Sensitivity Analysis

Effect of λ_c . We conduct experiments on the 2D-to-3D task of $USA \rightarrow Sing.$ via the bridge domain A2D2 to study the effect of λ_c . According to Figure 3, LSB is insensitive to a wide range of $\lambda_c \in [1, 10]$. Notably, LSB performs worse than LSB (w.o \mathcal{L}_{con}^b) when $\lambda_c < 0.1$, showing that a small λ_c is not suitable for LSB to learn a consistent feature.

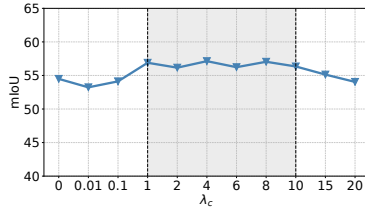


Figure 3: Effect of λ_c .

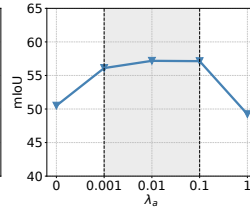


Figure 4: Effect of λ_a .

Effect of λ_a . To investigate the sensitivity of λ_a , we conduct the experiments on the $USA \rightarrow Sing.$ task. Figure 4 shows the testing mIoU w.r.t. λ_a . As can be seen, LSB achieves good performance in the range of $\lambda_a \in [0.001, 0.1]$. Moreover, increasing λ_a can boost mIoU when λ_a is small. However, excessively large values of λ_a lead to a significant performance drop.

6 Conclusion

In this paper, we introduce HMUDA, a novel setting designed to transfer knowledge between heterogeneous modalities using a bridge domain. For HMUDA, we propose a specialized framework LSB, with two distinct networks tailored for the source and target modalities. These networks are trained jointly with two segmentation losses specific to each network, alongside a feature consistency loss to promote similar feature representations between networks and a domain alignment loss to reduce domain discrepancies. Experimental results on various HMUDA benchmark datasets demonstrate the effectiveness of LSB in transferring knowledge across heterogeneous modalities. In our future work, we will apply LSB to other HMUDA tasks, such as image classification and object detection.

References

- [1] F. LastName, “The frobnicatable foo filter,” 2014, face and Gesture submission ID 324. Supplied as supplemental material fg324.pdf.
- [2] F. Alpher, “Frobnication,” *IEEE TPAMI*, vol. 12, no. 1, pp. 234–778, 2002.
- [3] F. Alpher and F. Fotheringham-Smythe, “Frobnication revisited,” *Journal of Foo*, vol. 13, no. 1, pp. 234–778, 2003.
- [4] F. Alpher, F. Fotheringham-Smythe, and F. Gamow, “Can a machine frobnicate?” *Journal of Foo*, vol. 14, no. 1, pp. 234–778, 2004.
- [5] F. Alpher and F. Gamow, “Can a computer frobnicate?” in *ICCV*, 2005, pp. 234–778.
- [6] H. Pham, Z. Dai, Q. Xie, and Q. V. Le, “Meta pseudo labels,” in *Proceedings of the IEEE/CVF Conference on Computer Vision and Pattern Recognition (CVPR)*, June 2021.
- [7] Y. Tang, W. Chen, Y. Luo, and Y. Zhang, “Humble teachers teach better students for semi-supervised object detection,” in *Proceedings of the IEEE/CVF Conference on Computer Vision and Pattern Recognition (CVPR)*, June 2021.
- [8] H. Caesar, V. Bankiti, A. H. Lang, S. Vora, V. E. Liong, Q. Xu, A. Krishnan, Y. Pan, G. Baldan, and O. Beijbom, “nuscenes: A multimodal dataset for autonomous driving,” in *Proceedings of the IEEE/CVF Conference on Computer Vision and Pattern Recognition (CVPR)*, June 2020.
- [9] A. Gaidon, Q. Wang, Y. Cabon, and E. Vig, “Virtual worlds as proxy for multi-object tracking analysis,” in *Proceedings of the IEEE Conference on Computer Vision and Pattern Recognition (CVPR)*, June 2016.
- [10] J. Behley, M. Garbade, A. Milioto, J. Quenzel, S. Behnke, C. Stachniss, and J. Gall, “Semantickitti: A dataset for semantic scene understanding of lidar sequences,” in *Proceedings of the IEEE/CVF International Conference on Computer Vision (ICCV)*, October 2019.
- [11] D. Peng, Y. Lei, W. Li, P. Zhang, and Y. Guo, “Sparse-to-dense feature matching: Intra and inter domain cross-modal learning in domain adaptation for 3d semantic segmentation,” in *Proceedings of the IEEE/CVF International Conference on Computer Vision (ICCV)*, October 2021.
- [12] J. Geyer, Y. Kassahun, M. Mahmudi, X. Ricou, R. Durgesh, A. S. Chung, L. Hauswald, V. H. Pham, M. Mühlegg, S. Dorn, T. Fernandez, M. Jänicke, S. Mirashi, C. Savani, M. Sturm, O. Vorobiov, M. Oelker, S. Garreis, and P. Schuberth, “A2D2: Audi Autonomous Driving Dataset,” 2020. [Online]. Available: <https://www.a2d2.audi>
- [13] K. Sohn, D. Berthelot, N. Carlini, Z. Zhang, H. Zhang, C. A. Raffel, E. D. Cubuk, A. Kurakin, and C.-L. Li, “Fixmatch: Simplifying semi-supervised learning with consistency and confidence,” *Advances in Neural Information Processing Systems*, vol. 33, pp. 596–608, 2020.
- [14] B. Zhang, Y. Wang, W. Hou, H. Wu, J. Wang, M. Okumura, and T. Shinozaki, “Flexmatch: Boosting semi-supervised learning with curriculum pseudo labeling,” *Advances in Neural Information Processing Systems*, vol. 34, pp. 18 408–18 419, 2021.
- [15] M. Jaritz, T.-H. Vu, R. De Charette, É. Wirbel, and P. Pérez, “Cross-modal learning for domain adaptation in 3d semantic segmentation,” *IEEE Transactions on Pattern Analysis and Machine Intelligence*, vol. 45, no. 2, pp. 1533–1544, 2022.
- [16] A. Tarvainen and H. Valpola, “Mean teachers are better role models: Weight-averaged consistency targets improve semi-supervised deep learning results,” *Advances in neural information processing systems*, vol. 30, 2017.
- [17] J. Deng, W. Dong, R. Socher, L.-J. Li, K. Li, and L. Fei-Fei, “Imagenet: A large-scale hierarchical image database,” in *2009 IEEE conference on computer vision and pattern recognition*. Ieee, 2009, pp. 248–255.
- [18] O. Ronneberger, P. Fischer, and T. Brox, “U-net: Convolutional networks for biomedical image segmentation,” in *Medical image computing and computer-assisted intervention—MICCAI 2015: 18th international conference, Munich, Germany, October 5-9, 2015, proceedings, part III 18*. Springer, 2015, pp. 234–241.
- [19] K. He, X. Zhang, S. Ren, and J. Sun, “Deep residual learning for image recognition,” in *Proceedings of the IEEE conference on computer vision and pattern recognition*, 2016, pp. 770–778.

- [20] B. Graham, M. Engelcke, and L. Van Der Maaten, “3d semantic segmentation with submanifold sparse convolutional networks,” in *Proceedings of the IEEE conference on computer vision and pattern recognition*, 2018, pp. 9224–9232.
- [21] M. Long, Y. Cao, J. Wang, and M. Jordan, “Learning transferable features with deep adaptation networks,” in *Proc. Int. Conf. Mach. Learn. (ICML)*, vol. 1. PMLR, 2015, pp. 97–105.
- [22] Y. Zhu, F. Zhuang, J. Wang, G. Ke, J. Chen, J. Bian, H. Xiong, and Q. He, “Deep subdomain adaptation network for image classification,” *IEEE Trans. Neural Netw. Learn. Syst.*, vol. 32, no. 4, pp. 1713–1722, 2021.
- [23] Y. Li, L. Yuan, and N. Vasconcelos, “Bidirectional learning for domain adaptation of semantic segmentation,” in *Proceedings of the IEEE/CVF conference on computer vision and pattern recognition*, 2019, pp. 6936–6945.
- [24] B. Wu, X. Zhou, S. Zhao, X. Yue, and K. Keutzer, “Squeezesegv2: Improved model structure and unsupervised domain adaptation for road-object segmentation from a lidar point cloud,” in *2019 international conference on robotics and automation (ICRA)*. IEEE, 2019, pp. 4376–4382.
- [25] B. Graham, M. Engelcke, and L. Van Der Maaten, “3d semantic segmentation with submanifold sparse convolutional networks,” in *Proceedings of the IEEE conference on computer vision and pattern recognition*, 2018, pp. 9224–9232.
- [26] Q. Hu, B. Yang, L. Xie, S. Rosa, Y. Guo, Z. Wang, N. Trigoni, and A. Markham, “Randla-net: Efficient semantic segmentation of large-scale point clouds,” in *Proceedings of the IEEE/CVF conference on computer vision and pattern recognition*, 2020, pp. 11 108–11 117.
- [27] S. Xie, J. Gu, D. Guo, C. R. Qi, L. Guibas, and O. Litany, “Pointcontrast: Unsupervised pre-training for 3d point cloud understanding,” in *Computer Vision—ECCV 2020: 16th European Conference, Glasgow, UK, August 23–28, 2020, Proceedings, Part III 16*. Springer, 2020, pp. 574–591.
- [28] M. Li, Y. Zhang, Y. Xie, Z. Gao, C. Li, Z. Zhang, and Y. Qu, “Cross-domain and cross-modal knowledge distillation in domain adaptation for 3d semantic segmentation,” in *Proceedings of the 30th ACM International Conference on Multimedia*, 2022, pp. 3829–3837.
- [29] J. Hoffman, E. Tzeng, T. Park, J.-Y. Zhu, P. Isola, K. Saenko, A. Efros, and T. Darrell, “Cycada: Cycle-consistent adversarial domain adaptation,” in *International conference on machine learning*. Pmlr, 2018, pp. 1989–1998.
- [30] Y. Zou, Z. Yu, X. Liu, B. Kumar, and J. Wang, “Confidence regularized self-training,” in *Proceedings of the IEEE/CVF international conference on computer vision*, 2019, pp. 5982–5991.
- [31] F. Zhang, J. Fang, B. Wah, and P. Torr, “Deep fusionnet for point cloud semantic segmentation,” in *Computer Vision—ECCV 2020: 16th European Conference, Glasgow, UK, August 23–28, 2020, Proceedings, Part XXIV 16*. Springer, 2020, pp. 644–663.
- [32] Z. Zhuang, R. Li, K. Jia, Q. Wang, Y. Li, and M. Tan, “Perception-aware multi-sensor fusion for 3d lidar semantic segmentation,” in *Proceedings of the IEEE/CVF international conference on computer vision*, 2021, pp. 16 280–16 290.
- [33] Y. Luo, L. Zheng, T. Guan, J. Yu, and Y. Yang, “Taking a closer look at domain shift: Category-level adversaries for semantics consistent domain adaptation,” in *Proceedings of the IEEE/CVF conference on computer vision and pattern recognition*, 2019, pp. 2507–2516.
- [34] C. Saltori, F. Galasso, G. Fiameni, N. Sebe, E. Ricci, and F. Poiesi, “Cosmix: Compositional semantic mix for domain adaptation in 3d lidar segmentation,” in *European Conference on Computer Vision*. Springer, 2022, pp. 586–602.
- [35] A. Xiao, J. Huang, D. Guan, F. Zhan, and S. Lu, “Transfer learning from synthetic to real lidar point cloud for semantic segmentation,” in *Proceedings of the AAAI conference on artificial intelligence*, vol. 36, no. 3, 2022, pp. 2795–2803.
- [36] M. Jaritz, T.-H. Vu, R. d. Charette, E. Wirbel, and P. Pérez, “xmuda: Cross-modal unsupervised domain adaptation for 3d semantic segmentation,” in *Proceedings of the IEEE/CVF conference on computer vision and pattern recognition*, 2020, pp. 12 605–12 614.
- [37] D. Peng, Y. Lei, W. Li, P. Zhang, and Y. Guo, “Sparse-to-dense feature matching: Intra and inter domain cross-modal learning in domain adaptation for 3d semantic segmentation,” in *Proceedings of the IEEE/CVF International Conference on Computer Vision*, 2021, pp. 7108–7117.

- [38] Y. Wu, M. Xing, Y. Zhang, Y. Xie, J. Fan, Z. Shi, and Y. Qu, “Cross-modal unsupervised domain adaptation for 3d semantic segmentation via bidirectional fusion-then-distillation,” in *Proceedings of the 31st ACM International Conference on Multimedia*, 2023, pp. 490–498.
- [39] T. Kreutz, J. Lemke, M. Mühlhäuser, and A. S. Guinea, “Lion-xa: Unsupervised domain adaptation via lidar-only cross-modal adversarial training,” in *2024 IEEE/RSJ International Conference on Intelligent Robots and Systems (IROS)*. IEEE, 2024, pp. 8875–8881.
- [40] Q. Yang, Y. Zhang, W. Dai, and S. J. Pan, *Transfer learning*. Cambridge, U.K.: Cambridge Univ. Press, 2020.
- [41] X. Gu, J. Sun, and Z. Xu, “Unsupervised and semi-supervised robust spherical space domain adaptation,” *IEEE Trans Pattern Anal. Mach. Intell.*, pp. 1–17, 2022.
- [42] S. Zhao, X. Yue, S. Zhang, B. Li, H. Zhao, B. Wu, R. Krishna, J. E. Gonzalez, A. L. Sangiovanni-Vincentelli, S. A. Seshia, and K. Keutzer, “A review of single-source deep unsupervised visual domain adaptation,” *IEEE Trans. Neural Netw. Learn. Syst.*, vol. 33, no. 2, pp. 473–493, 2022.
- [43] M. Cordts, M. Omran, S. Ramos, T. Rehfeld, M. Enzweiler, R. Benenson, U. Franke, S. Roth, and B. Schiele, “The cityscapes dataset for semantic urban scene understanding,” in *Proceedings of the IEEE conference on computer vision and pattern recognition*, 2016, pp. 3213–3223.
- [44] Y. Guo, Y. Liu, T. Georgiou, and M. S. Lew, “A review of semantic segmentation using deep neural networks,” *International journal of multimedia information retrieval*, vol. 7, pp. 87–93, 2018.
- [45] R. Cheng, R. Razani, E. Taghavi, E. Li, and B. Liu, “2-s3net: Attentive feature fusion with adaptive feature selection for sparse semantic segmentation network,” in *Proceedings of the IEEE/CVF conference on computer vision and pattern recognition*, 2021, pp. 12 547–12 556.
- [46] H. Tang, Z. Liu, S. Zhao, Y. Lin, J. Lin, H. Wang, and S. Han, “Searching efficient 3d architectures with sparse point-voxel convolution,” in *European conference on computer vision*. Springer, 2020, pp. 685–702.
- [47] X. Yan, J. Gao, C. Zheng, C. Zheng, R. Zhang, S. Cui, and Z. Li, “2dpass: 2d priors assisted semantic segmentation on lidar point clouds,” in *European conference on computer vision*. Springer, 2022, pp. 677–695.
- [48] W. Liu, Z. Luo, Y. Cai, Y. Yu, Y. Ke, J. M. Junior, W. N. Gonçalves, and J. Li, “Adversarial unsupervised domain adaptation for 3d semantic segmentation with multi-modal learning,” *ISPRS Journal of Photogrammetry and Remote Sensing*, vol. 176, pp. 211–221, 2021.
- [49] Q. Xiao, Y. Zhang, and Q. Yang, “Selective random walk for transfer learning in heterogeneous label spaces,” *IEEE Transactions on Pattern Analysis and Machine Intelligence*, vol. 46, no. 6, pp. 4476–4488, 2024.
- [50] R. Strudel, R. Garcia, I. Laptev, and C. Schmid, “Segmenter: Transformer for semantic segmentation,” in *Proceedings of the IEEE/CVF international conference on computer vision*, 2021, pp. 7262–7272.
- [51] L. Li, T. Zhou, W. Wang, J. Li, and Y. Yang, “Deep hierarchical semantic segmentation,” in *Proceedings of the IEEE/CVF Conference on Computer Vision and Pattern Recognition*, 2022, pp. 1246–1257.
- [52] Z. Fang, J. Lu, F. Liu, and G. Zhang, “Semi-supervised heterogeneous domain adaptation: Theory and algorithms,” *IEEE Transactions on Pattern Analysis and Machine Intelligence*, vol. 45, no. 1, pp. 1087–1105, 2022.
- [53] C. Wang and S. Mahadevan, “Heterogeneous domain adaptation using manifold alignment,” in *IJCAI proceedings-international joint conference on artificial intelligence*, vol. 22, no. 1. Citeseer, 2011, p. 1541.
- [54] E. Tzeng, J. Hoffman, N. Zhang, K. Saenko, and T. Darrell, “Deep domain confusion: Maximizing for domain invariance,” *arXiv preprint arXiv:1412.3474*, 2014.
- [55] B. Sun and K. Saenko, “Deep coral: Correlation alignment for deep domain adaptation,” in *Computer vision—ECCV 2016 workshops: Amsterdam, the Netherlands, October 8–10 and 15–16, 2016, proceedings, part III 14*. Springer, 2016, pp. 443–450.
- [56] Y. Ganin, E. Ustinova, H. Ajakan, P. Germain, H. Larochelle, F. Laviolette, M. March, and V. Lempitsky, “Domain-adversarial training of neural networks,” *Journal of machine learning research*, vol. 17, no. 59, pp. 1–35, 2016.

- [57] E. Tzeng, J. Hoffman, K. Saenko, and T. Darrell, “Adversarial discriminative domain adaptation,” in *Proceedings of the IEEE conference on computer vision and pattern recognition*, 2017, pp. 7167–7176.
- [58] Y.-H. Tsai, W.-C. Hung, S. Schulter, K. Sohn, M.-H. Yang, and M. Chandraker, “Learning to adapt structured output space for semantic segmentation,” in *Proceedings of the IEEE conference on computer vision and pattern recognition*, 2018, pp. 7472–7481.
- [59] M. Long, H. Zhu, J. Wang, and M. I. Jordan, “Unsupervised domain adaptation with residual transfer networks,” *Advances in neural information processing systems*, vol. 29, 2016.
- [60] —, “Deep transfer learning with joint adaptation networks,” in *International conference on machine learning*. PMLR, 2017, pp. 2208–2217.
- [61] S. Shekhar, V. M. Patel, H. V. Nguyen, and R. Chellappa, “Generalized domain-adaptive dictionaries,” in *Proceedings of the IEEE conference on computer vision and pattern recognition*, 2013, pp. 361–368.
- [62] L. Duan, D. Xu, and I. Tsang, “Learning with augmented features for heterogeneous domain adaptation,” *arXiv preprint arXiv:1206.4660*, 2012.
- [63] J. Zhang, W. Li, and P. Ogunbona, “Joint geometrical and statistical alignment for visual domain adaptation,” in *Proceedings of the IEEE conference on computer vision and pattern recognition*, 2017, pp. 1859–1867.
- [64] L. Shao, F. Zhu, and X. Li, “Transfer learning for visual categorization: A survey,” *IEEE transactions on neural networks and learning systems*, vol. 26, no. 5, pp. 1019–1034, 2014.
- [65] O. Day and T. M. Khoshgoftaar, “A survey on heterogeneous transfer learning,” *Journal of Big Data*, vol. 4, pp. 1–42, 2017.
- [66] M. Wang and W. Deng, “Deep visual domain adaptation: A survey,” *Neurocomputing*, vol. 312, pp. 135–153, 2018.
- [67] D. R. Hardoon, S. Szedmak, and J. Shawe-Taylor, “Canonical correlation analysis: An overview with application to learning methods,” *Neural computation*, vol. 16, no. 12, pp. 2639–2664, 2004.
- [68] A. Samat, C. Persello, P. Gamba, S. Liu, J. Abuduwaili, and E. Li, “Supervised and semi-supervised multi-view canonical correlation analysis ensemble for heterogeneous domain adaptation in remote sensing image classification,” *Remote sensing*, vol. 9, no. 4, p. 337, 2017.
- [69] Y.-H. H. Tsai, Y.-R. Yeh, and Y.-C. F. Wang, “Learning cross-domain landmarks for heterogeneous domain adaptation,” in *Proceedings of the IEEE conference on computer vision and pattern recognition*, 2016, pp. 5081–5090.
- [70] J. T. Zhou, I. W. Tsang, S. J. Pan, and M. Tan, “Heterogeneous domain adaptation for multiple classes,” in *Artificial intelligence and statistics*. PMLR, 2014, pp. 1095–1103.
- [71] B. Kulis, K. Saenko, and T. Darrell, “What you saw is not what you get: Domain adaptation using asymmetric kernel transforms,” in *CVPR 2011*. IEEE, 2011, pp. 1785–1792.
- [72] K. D. Feuz and D. J. Cook, “Transfer learning across feature-rich heterogeneous feature spaces via feature-space remapping (fsr),” *ACM transactions on intelligent systems and technology (TIST)*, vol. 6, no. 1, pp. 1–27, 2015.
- [73] Y. Luo, P. Liu, T. Guan, J. Yu, and Y. Yang, “Significance-aware information bottleneck for domain adaptive semantic segmentation,” in *Proceedings of the IEEE/CVF international conference on computer vision*, 2019, pp. 6778–6787.
- [74] Y. Mo, Y. Wu, X. Yang, F. Liu, and Y. Liao, “Review the state-of-the-art technologies of semantic segmentation based on deep learning,” *Neurocomputing*, vol. 493, pp. 626–646, 2022.
- [75] Y. Zhang, M. Li, Y. Xie, C. Li, C. Wang, Z. Zhang, and Y. Qu, “Self-supervised exclusive learning for 3d segmentation with cross-modal unsupervised domain adaptation,” in *Proceedings of the 30th ACM International Conference on Multimedia*, 2022, pp. 3338–3346.
- [76] Y. Wu, M. Xing, Y. Zhang, Y. Xie, and Y. Qu, “Clip2uda: Making frozen clip reward unsupervised domain adaptation in 3d semantic segmentation,” in *Proceedings of the 32nd ACM International Conference on Multimedia*, 2024, pp. 8662–8671.
- [77] M. Xiao and Y. Guo, “Feature space independent semi-supervised domain adaptation via kernel matching,” *IEEE transactions on pattern analysis and machine intelligence*, vol. 37, no. 1, pp. 54–66, 2014.

- [78] J. Zhou, S. Pan, I. Tsang, and Y. Yan, “Hybrid heterogeneous transfer learning through deep learning,” in *Proceedings of the AAAI Conference on Artificial Intelligence*, vol. 28, no. 1, 2014.
- [79] J. Nam and S. Kim, “Heterogeneous defect prediction,” in *Proceedings of the 2015 10th joint meeting on foundations of software engineering*, 2015, pp. 508–519.
- [80] F. Zhuang, Z. Qi, K. Duan, D. Xi, Y. Zhu, H. Zhu, H. Xiong, and Q. He, “A comprehensive survey on transfer learning,” *Proceedings of the IEEE*, vol. 109, no. 1, pp. 43–76, 2020.
- [81] A. Kirillov, E. Mintun, N. Ravi, H. Mao, C. Rolland, L. Gustafson, T. Xiao, S. Whitehead, A. C. Berg, W.-Y. Lo *et al.*, “Segment anything,” in *Proceedings of the IEEE/CVF international conference on computer vision*, 2023, pp. 4015–4026.
- [82] S. Ben-David, J. Blitzer, K. Crammer, A. Kulesza, F. Pereira, and J. W. Vaughan, “A theory of learning from different domains,” *Machine learning*, vol. 79, pp. 151–175, 2010.
- [83] B. Zhou, H. Zhao, X. Puig, S. Fidler, A. Barriuso, and A. Torralba, “Scene parsing through ade20k dataset,” in *Proceedings of the IEEE conference on computer vision and pattern recognition*, 2017, pp. 633–641.
- [84] H. Caesar, J. Uijlings, and V. Ferrari, “Coco-stuff: Thing and stuff classes in context,” in *Proceedings of the IEEE conference on computer vision and pattern recognition*, 2018, pp. 1209–1218.
- [85] G. Neuhold, T. Ollmann, S. Rota Bulò, and P. Kotschieder, “The mapillary vistas dataset for semantic understanding of street scenes,” in *Proceedings of the IEEE international conference on computer vision*, 2017, pp. 4990–4999.
- [86] Z. Zhuang, Y. Zhang, and Y. Wei, “Gradual domain adaptation via gradient flow,” in *The Twelfth International Conference on Learning Representations*, 2024.

A The overall algorithm for the LSB method

Algorithm 1 The LSB method.

Require: Source domain \mathcal{S} , target domain \mathcal{T} , bridge domain \mathcal{B} , learning rate η , hyper-parameters λ_c and λ_a ; trainable parameters θ : source network $\{h, f\}$, target network $\{\phi, g\}$ and projections $\{p_h, p_\phi\}$;

- 1: **repeat**
- 2: Initialize the source teacher model $\{\hat{h}, \hat{f}\}$.
- 3: Sample a batch of data $\tilde{\mathcal{S}} \subset \mathcal{S}, \tilde{\mathcal{B}} \subset \mathcal{B}, \tilde{\mathcal{T}} \subset \mathcal{T}$.
- 4: **for** $(\mathbf{x}^s, \mathbf{y}^s) \in \tilde{\mathcal{S}}$ **do**
- 5: Compute loss $\mathcal{L}_{\text{seg}}^s(\mathbf{x}^s, \mathbf{y}^s)$ by Eq. (1).
- 6: **end for**
- 7: **for** $(\mathbf{x}^{bs}, \mathbf{x}^{bt}) \in \tilde{\mathcal{B}}$ **do**
- 8: Compute loss $\mathcal{L}_{\text{seg}}^b(\mathbf{x}^{bs}, \mathbf{x}^{bt})$ by Eq. (5).
- 9: Compute loss $\mathcal{L}_{\text{con}}^b(\mathbf{x}^{bs}, \mathbf{x}^{bt})$ by Eq. (6).
- 10: **end for**
- 11: Compute loss $\mathcal{L}_{\text{ali}}(\tilde{\mathcal{S}}, \tilde{\mathcal{T}})$ by Eq. (9).
- 12: Compute the overall loss \mathcal{L} by Eq. (10).
- 13: $\theta \leftarrow \theta - \eta \nabla_{\theta} \mathcal{L}$;
- 14: Update $\{\hat{h}, \hat{f}\}$ using EMA from $\{h, f\}$ by Eq. (2).
- 15: **until** convergence

B Proof of Theorem 1

Proof. This proof relies on Theorem 2 in [82]. We begin with the following inequality:

$$\mathcal{E}_{bs}(\{h, f\}) \leq \mathcal{E}_s(\{h, f\}) + \frac{1}{2} (d_{\mathcal{H}_s \Delta \mathcal{H}_s}(\mathcal{D}_s, \mathcal{D}_b)) + \lambda_s \quad (15)$$

and

$$\begin{aligned} \mathcal{E}_t(\{\phi, g\}) &\leq \mathcal{E}_{bt}(\{\phi, g\}) + \frac{1}{2} (d_{\mathcal{H}_t \Delta \mathcal{H}_t}(\mathcal{D}_b, \mathcal{D}_t)) + \lambda_t \\ &\leq \mathcal{E}_{bs}(\{h, f\}) + \mathcal{E}_{bt}(\{\phi, g\}) - \mathcal{E}_{bs}(\{h, f\}) + \frac{1}{2} (d_{\mathcal{H}_t \Delta \mathcal{H}_t}(\mathcal{D}_b, \mathcal{D}_t)) + \lambda_t \\ &\leq \mathcal{E}_{bs}(\{h, f\}) + |\mathcal{E}_{bt}(\{\phi, g\}) - \mathcal{E}_{bs}(\{h, f\})| + \frac{1}{2} (d_{\mathcal{H}_t \Delta \mathcal{H}_t}(\mathcal{D}_b, \mathcal{D}_t)) + \lambda_t, \end{aligned} \quad (16)$$

According to the modality assumption, we have:

$$|\mathcal{E}_{bt}(\{\phi, g\}) - \mathcal{E}_{bs}(\{h, f\})| \leq L \mathbb{E}_{(\mathbf{x}^{bs}, \mathbf{x}^{bt}) \sim \mathcal{D}_b} (d(h(\mathbf{x}^{bs}), \phi(\mathbf{x}^{bt}))) \quad (17)$$

By combining inequalities (15), (16) and (17), we obtain:

$$\begin{aligned} \mathcal{E}_t(\{\phi, g\}) &\leq \mathcal{E}_{bs}(\{h, f\}) + |\mathcal{E}_{bt}(\{\phi, g\}) - \mathcal{E}_{bs}(\{h, f\})| + \frac{1}{2} (d_{\mathcal{H}_t \Delta \mathcal{H}_t}(\mathcal{D}_b, \mathcal{D}_t)) + \lambda_t \\ &\leq \mathcal{E}_{bs}(\{h, f\}) + L \mathbb{E}_{(\mathbf{x}^{bs}, \mathbf{x}^{bt}) \sim \mathcal{D}_b} (d(h(\mathbf{x}^{bs}), \phi(\mathbf{x}^{bt}))) + \frac{1}{2} (d_{\mathcal{H}_t \Delta \mathcal{H}_t}(\mathcal{D}_b, \mathcal{D}_t)) + \lambda_t \\ &\leq \mathcal{E}_s(\{h, f\}) + L \mathbb{E}_{(\mathbf{x}^{bs}, \mathbf{x}^{bt}) \sim \mathcal{D}_b} (d(h(\mathbf{x}^{bs}), \phi(\mathbf{x}^{bt}))) + (\lambda_s + \lambda_t) \\ &\quad + \frac{1}{2} (d_{\mathcal{H}_s \Delta \mathcal{H}_s}(\mathcal{D}_s, \mathcal{D}_b)) + \frac{1}{2} (d_{\mathcal{H}_t \Delta \mathcal{H}_t}(\mathcal{D}_b, \mathcal{D}_t)), \end{aligned} \quad (18)$$

□

C Detailed Experimental Settings

Datasets We construct eight HMUDA scenarios based on four datasets. Table 6 shows the details of each scenario.

Scenario	\mathcal{B}		\mathcal{S}		\mathcal{T}	
		Train	Train	Train	Val/Test	
<i>USA</i> \rightarrow <i>Sing.</i>	Sem.	18,029	15,695	9,665	2,770/2,929	
<i>Day</i> \rightarrow <i>Night</i>			24,745	2,779	602/602	
<i>Virt.</i> \rightarrow <i>A2D2</i>			2,126	22,420	1,318/3,956	
<i>USA</i> \rightarrow <i>Sing.</i>	A2D2	22,420	15,695	9,665	2,770/2,929	
<i>Day</i> \rightarrow <i>Night</i>			24,745	2,779	602/602	
<i>Virt.</i> \rightarrow <i>Sem.</i>			2,126	18,029	1,101/4,071	
<i>Sem.</i> \rightarrow <i>A2D2</i>	Virt.	2,126	18,029	22,420	1,318/3,956	
<i>A2D2</i> \rightarrow <i>Sem.</i>			22,420	18,029	1,101/4,071	

Table 6: The sample number in each split of datasets for all eight settings. Note that the training samples in target and bridge domains are without labels.

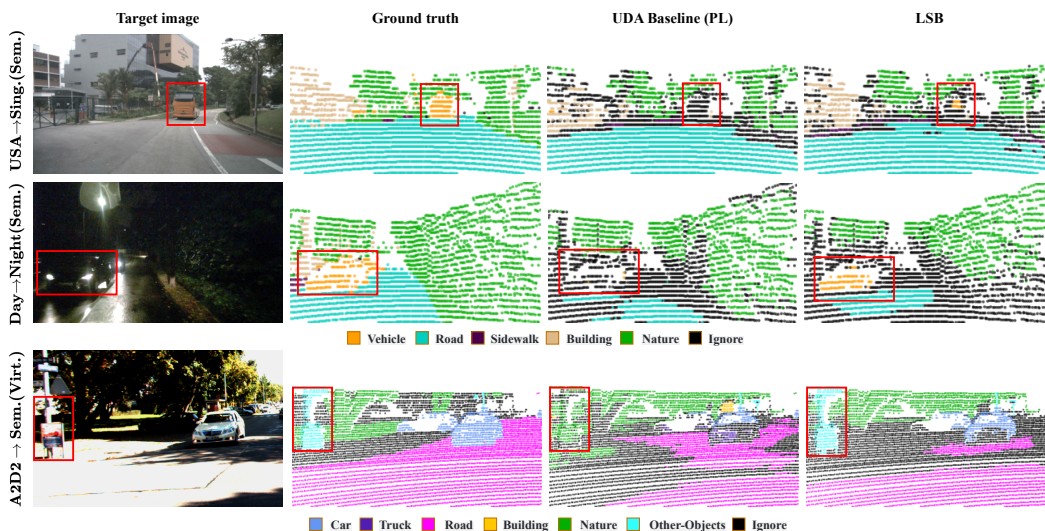


Figure 5: Qualitative results on three 2D-to-3D HMUDA tasks: *USA* \rightarrow *Sing.*, *Day* \rightarrow *Night*, and *A2D2* \rightarrow *Sem.*. The (\cdot) in the vertical axis denotes the bridge domain \mathcal{B} used in the HMUDA task. For example, **USA** \rightarrow **Sing.(Sem.)** denotes the transfer from *USA* to *Sing.* via the bridge domain *Sem.*.

D Visualization

Figure 5 presents the qualitative segmentation results for various 2D-to-3D tasks, including *USA* \rightarrow *Sing.*, *Day* \rightarrow *Night*, and *A2D2* \rightarrow *Sem.*. As can be seen, the LSB method predicts segmentation objects more accurately than the baseline method (PL). For instance, in the *USA* \rightarrow *Sing.* task, buses are highlighted with red bounding boxes. We can see that the proposed LSB method correctly identifies the bus, while the baseline method PL misclassifies these points as ‘Sidewalk’. Similar improvements are observed in the *Day* \rightarrow *Night* and *A2D2* \rightarrow *Sem.* tasks, where LSB effectively recognizes ‘Vehicle’ and ‘Other-Objects’.

E Limitations

This work focuses on establishing a novel unsupervised domain adaptation framework for heterogeneous modalities, while in application, we only evaluate the vision-based modalities, i.e., 2D images and 3D point clouds. In our future work, we will apply LSB to other HMUDA tasks, such as image classification and object detection.